Eur. J. Mech., B/Fluids, **17,** n° 1, 51-77, 1998

Wetting prevention by thermal Marangoni effect. Experimental and numerical simulation

R. MONTI [a], R. SAVINO [b] and S. TEMPESTA

ABSTRACT. – The behaviour of small liquid drops, hanging from a circular disk and approaching a flat wall at a different temperature is studied experimentally and numerically. If the pendant drop and the solid surface are at the same temperature and if the liquid wets the solid, the drop spreads over the surface forming a liquid bridge in times of the order of milliseconds. If the upper disk is heated and/or the solid surface is cooled, then the drop does not wet the wall, even if pressed against the surface, but it is deformed in a completely reversible way, similarly to an elastic material (e.g. like a rubber balloon).

To investigate this unusual and intriguing phenomenon, a systematic experimental programme has been carried out on silicone oils (with different viscosities) and on diesel oils. At the same time the problem was studied numerically under the assumption that a thin air film exists between the drop and the solid surface. This film is formed by the entrainment of the surrounding air caused by the Marangoni flow directed, along the liquid surface, from the upper disk towards the contact zone. If suitable conditions are established, the pressure in the air film balances the pressure necessary to deform the liquid drop, preventing the wetting of the solid surface. The experimental results agree with the proposed numerical model. In particular the computed equilibrium air film thicknesses are compared with the thicknesses measured with a background illumination system and with an interferometric technique; a good agreement is found between numerical and experimental results, for different liquids and different geometrical configurations. © Elsevier, Paris.

1. Introduction

The behaviour of a pendant drop approaching a solid surface at a different temperature is important in many engineering applications. This is the configuration used to evaluate the wetting of a surface by a liquid, especially in the processes of soldering or brazing (Ambrose *et al.*, 1996; Yost *et al.*, 1993). While there is not a direct correlation between the wettability of a solder and the quality of the joint, good wetting is an essential prerequisite for the formation of a solder joint. This problem has been the subject of research; a review article on the spreading of drops on solids surfaces has been given by Dussan (1979); other experimental or numerical studies dealing with spreading of liquids on solids are those of Ehrard and Davis (1991), Ehrard (1993), Anderson and Davis (1995) and Smith (1995). Numerical simulations of the spreading of liquid drops over

Università degli Studi di Napoli "Federico II", Dipartimento di Scienza e Ingegneria dello Spazio "Luigi G. Napolitano", P.le V.Tecchio 80, 80125 Napoli, Italy.

[a] E-mail: monti@unina.it

[b] E-mail: rasavino@unina.it

0997-7546/98/01/© Elsevier, Paris

solid surfaces, in the presence of gravity and capillary effects induced by temperature and concentration gradients, have been presented by Braun *et al.* (1995).

Other engineering applications for studying this problem are in the field of diesel engine combustion, where a number of injected liquid droplets arrive at the cylinder walls before ignition.

Interactions between drops and solid surfaces occur also during solidification processes, when one or more liquid inclusions arrive at a solidification front maintained at temperature lower than the surrounding melt temperature (Gao and Sonin, 1994; Trapaga *et al.*, 1992; Fukai *et al.*, 1993, 1995).

Following previous research studies on the behaviour of two non coalescing drops of the same liquid (Monti, Savino and Cicala, 1996; Savino and Monti, 1997; Monti and Savino, 1996, 1997), a number of experiments have been performed at the Department of Space Science and Engineering of Naples University to investigate the unusual behaviour that drops of different liquid (e.g. silicone oils and diesel oils) exhibit when put in contact with a solid surface maintained at a different temperature. The properties of the tested liquids are shown in Table I. In particular, the prevention of the liquid wetting, observed when the liquid drop is heated with respect to the horizontal plane, has been explained introducing a fluid-dynamic model based on the assumption that a thin air film, separating the drop from the solid surface, is formed by the entrainment action induced by the Marangoni velocities along the liquid surface.

TABLE I. – Physical properties of the liquids investigated.

	ρ [g/cm^3]	ν [cm^2/s]	α [cm^2/s]	σ [dyne/cm]	σ_T [dyne/cmK]	T_b (°C)	T_m (°C)
Silicon oil 2 cs	0.872	0.02	0.00058	18.7	0.06	80	- 84
Silicon oil 5 cs	0.91	0.05	0.00065	19.7	0.06	136	- 65
Silicon oil 100 cs	0.965	1	0.00112	20.9	0.06	> 300	- 55
Diesel oil	0.82-0.84	0.014-0.05	0.072-0.081	25-30	0.013	180-340	- 10

In this paper we report the results of the experimental investigation and of the numerical simulations. Section 2 of this paper deals with the experimental analysis. The experimental apparatus and the qualitative behaviour observed during the experiments are described in paragraphs 2.1 and 2.2. The experimental procedure is illustrated in paragraph 2.3, together with results concerning the critical temperature differences measured for the different configurations under study.

Two different techniques used for the measurement of the air film, separating the liquid drop from the solid surface, are illustrated in paragraph 2.4.

Section 3 deals with the fluid-dynamic model, including the free boundary value problem for the liquid drop surface, the Navier-Stokes equations for the liquid and for the air phases, and the appropriate boundary and symmetry conditions.

The numerical results are discussed in paragraph 3.2. The comparison between the experimental and numerical results is presented in Section 4. Concluding remarks are reported in Section 5.

2. Experimental analysis

2.1. Description of the experimental apparatus

A general scheme of the experimental apparatus is illustrated in Figure 1. The facility includes a mechanical support system, a temperature control system and a visualisation system. The support system is a cylindrical copper disk (2) sustaining a liquid drop (1). This disk can be translated along the vertical axis, changing the relative distance between the drop and the horizontal plane.

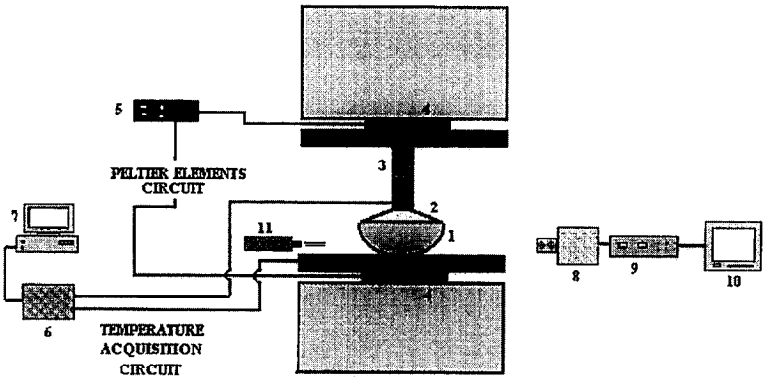

Fig. 1. – Scheme of the experimental apparatus. (1): drop; (2): copper disk; (3): copper cylinder; (4): Peltier elements; (5): AC/CD; (6): A/D converter; (7): personal computer; (8): camera CCD; (9): video recorder; (10): monitor; (11): laser.

The temperature control system includes two Peltier elements (4) able to establish and control appropriate temperatures on the disk and on the solid surface, so that an arbitrary temperature difference between the drop and the plane can be imposed.

Two temperature sensors, located on the disk and on the solid surface, are connected with a personal computer (7) by means of an analog/digital (A/D) converter (6). The temperature can be measured with an accuracy of $\pm$ 0.02 K.

The motion inside the liquid drops is evaluated by visualizing tracers added to the liquid (hollow glass microspheres with diameter ranging from 2 to 20 μm) illuminated by a laser light cut in the meridian plane. A CCD camera (8) and a video recorder (9) are used to film and record the video images.

2.2. Behaviour of a liquid drop approaching a solid surface

A pendant liquid drop is formed on the circular disk and is moved towards the solid surface by translating the disk downwards. When the disk and the horizontal surface are at the same temperature (ambient temperature) no motion arises in the liquid drop, as shown in Figure 2 *a* (motionless tracers); at these conditions, if the drop is put in contact to the wall, by moving the disk down, the liquid spreads over the solid surface forming a liquid bridge in times of the order of milliseconds (*Fig. 2 b*).

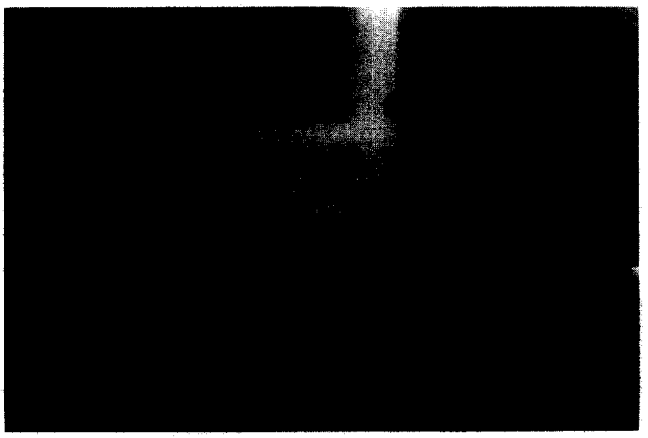

(*a*)

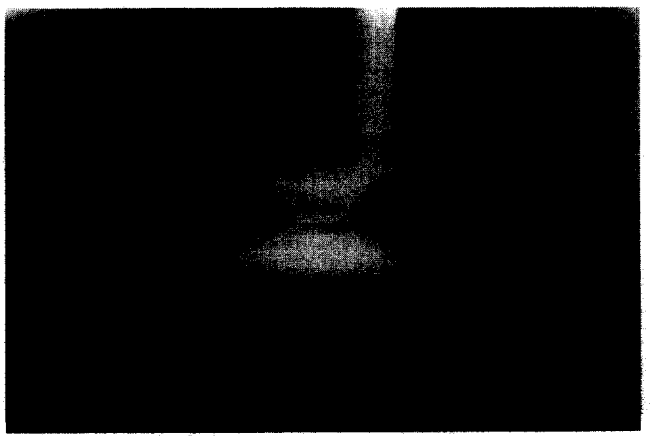

(*b*)

Fig. 2. – Photographs illustrating the liquid drop behaviour in the isothermal situation.

If this experimental sequence is repeated after establishing a temperature difference between the disk and the horizontal surface (by heating the pendant drop and/or by cooling the solid wall with respect to the ambient temperature), then Marangoni flows will appear inside the liquid drop, due to the surface tension unbalance induced by the surface temperature differences (*Fig.* 3 *a*). In particular, since the surface tension is a decreasing function of the temperature, the velocity along the drop surface is downward (opposite to the imposed temperature gradient), *i.e.* directed from the upper disk to the region of contact between the drop and the solid surface. By continuity, the flow inside the drop close to the symmetry axis is directed from the contact region towards the upper disk. When the drop is now slowly brought in contact with the surface, if the temperature difference is sufficiently large (of the order of few degrees centigrade), no wetting occurs (*Fig.* 3 *b*). If the drop is pressed against the solid surface, it is deformed in a completely reversible way, similarly to an elastic balloon (*Figs.* 3 *c*, *d*).

(*a*)

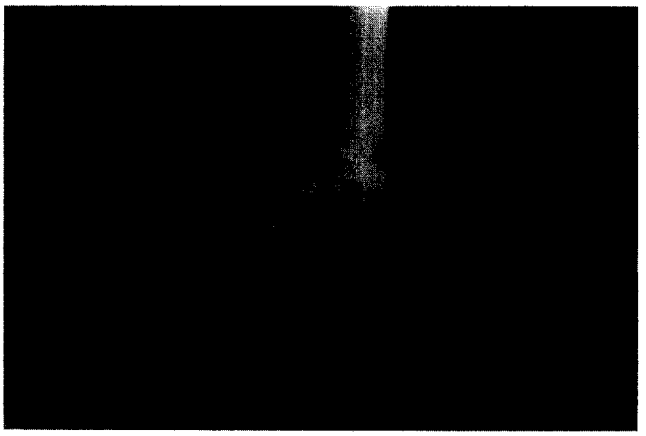

(*b*)

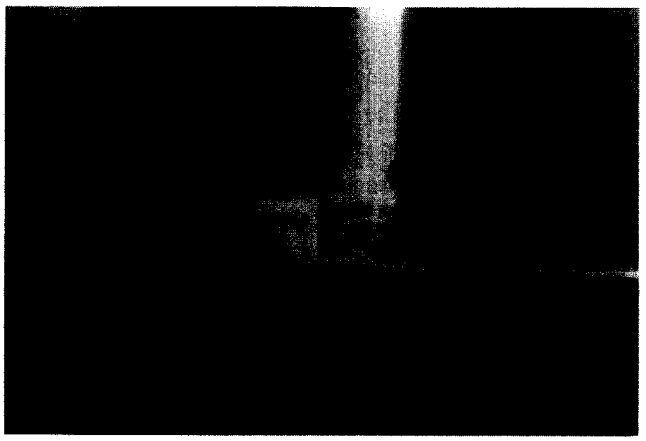

(*c*)

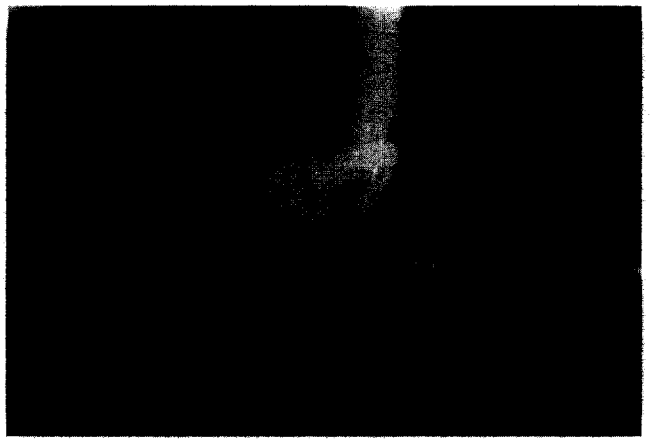

(*d*)

Fig. 3. – Photographs illustrating the liquid drop behaviour for $\Delta T = 25$ K (the disk is hot and the wall cold).

If the temperature gradient is reversed (by cooling the disk and/or by heating the solid surface), then the Marangoni flow is reversed and is directed from the contact region to the solid support (along the liquid drop surface) and when the drop contacts the solid surface the liquid spreads over the solid surface (as in the isothermal situation).

To explain the absence of wetting observed when the drop is warmer than the wall surface, a fluid-dynamic model is formulated, based on the assumption that a thin air film is formed between the liquid drop and the solid surface, due to the fact that Marangoni flows convect ambient air to form an air film. A similar assumption is made to explain the unusual behaviour observed when two drops of the same liquid are contacted in the presence of surface tension-driven flows induced by temperature differences; the drops can be pressed and even squeezed against each other (no coalescence occurs) (Savino and Monti, 1997; Monti and Savino, 1996, 1997).

The model of the separating air film, for the drop-wall system that prevents wetting, can be summarized as follows. For wetting to occur the thin air film that separates the surface of the liquid drop from the wall must be removed so that the liquid could come into molecular contact with the surface. If the hanging drop is hot and the wall is cold, then the Marangoni flow along the drop surface is directed from the upper disk to the contact region and the ambient air surrounding the surface of the drop is entrained between the two surfaces. The pressure in the air film changes from the ambient to a maximum value in correspondence of the axis of symmetry. This pressure increase is needed to balance the surface force necessary to deform the drop from a hemispherical shape to a flattened shape such as that shown in Figure 3 *c*.

2.3. Experimental procedure for the measurement of the critical temperature differences

Laboratory experiments have been performed to evaluate the minimum value of the temperature difference (referred to as the critical temperature difference, ΔT_c) that must

be imposed between the drop and the solid surface to prevent the wetting of the solid surface, for given drop deformations.

The experimental sequence is illustrated below. A relatively large temperature difference is imposed, at this condition the drop can be pressed against the surface producing a flattening of the contact interface. It is left in this position and the temperature difference is progressively reduced (with a sufficiently small temperature ramp, in order to minimize unsteady effects); when the temperature difference reaches a critical value (ΔT_c), the liquid spreads over the solid and a liquide bridge is formed. The critical temperature difference is a function of the liquid properties, of the drop deformation and of the roughness and of the material of the solid surface. Table II reports the experimental results obtained using silicone oils drops with different viscosities, in contact with a glass (or copper) surface, for different values of the imposed pressure corresponding to different drop deformations. The initial drop radius is 1 mm; the deformations of the drops can be correlated to the pressure jump across the liquid drop surface by the numerical model described in Section 3. In particular, if σ is the surface tension and Δp the pressure jump across the curved portion of the drop surface (the pressure difference between the pressure inside the drop, assumed constant, and the ambient pressure), three different configurations have been studied: $\Delta p\, R/\sigma = 2.1$ (*Tab.* II *a*), $\Delta p\, R/\sigma = 2.4$ (*Tab.* II *b*), $\Delta p\, R/\sigma = 2.8$ (*Tab.* II *c*).

The results summarized in Table II can be interpreted according to the air film theory. In fact, for a prescribed value of the temperature difference and for a given drop deformation, the Marangoni surface velocities are smaller when the viscosity of the liquid is large (the characteristic velocity is $\sigma_T\, \Delta T/\mu$). For this reason the measured critical temperature differences (ΔT_c) in the case of a liquid drop of silicone oil 2 cs, are smaller than those corresponding to a viscosity 5 cs, whereas for a liquid drop of silicone oil 100 cs wetting occurs for all the values of the imposed temperature difference (up to 70°C). The values of the critical temperature difference (ΔT_c) are almost the same for solid surfaces made of glass or of copper. However, if the roughness of the surfaces increases, the critical temperature difference is larger because for a thin air film to prevent the contact between liquid and solid, the roughness size of the surface must be less than the thickness of the air film.

Table III summarises the experimental results obtained with diesel oils provided by different suppliers and a copper surface. The deformation of the drops corresponds to a dimensionless pressure jump $\Delta p\, R/\sigma = 2.8$.

The diesel fuel provided by the same company exhibits a different behaviour during different periods of the year. This may depend on the presence or the absence of anti-freeze. It is obvious that only a change of the surface tension derivative σ_T could explain the different intensities of the Marangoni convection. We plan to do future measurements of the surface tension at different temperatures to evaluate the σ_T in the presence or in the absence of anti-freeze to check if this assumption is correct.

2.4. Measurement of the air film thickness

To evaluate the thickness of the air film separating the liquid drop from the solid surface two experimental techniques have been implemented: a) a direct visualisation of

TABLE II. – Measured critical temperature differences for silicone oils with different viscosities in contact with a glass or a copper surface, for $\Delta p\, R/\sigma = 2.1$ (*a*), $\Delta p\, R/\sigma = 2.4$ (*b*), and $\Delta p\, R/\sigma = 2.8$ (*c*).

(*a*) $\Delta p\, R/\sigma = 2.1$

Viscosity of the silicone oil drop	Solid surface	ΔT_c [K] (Wetting)
2 cs	glass	1.0
	copper	1.3
5 cs	glass	1.4
	copper	1.6
100 cs	glass	> 70
	copper	> 70

(*b*) $\Delta p\, R/\sigma = 2.4$

Viscosity of the silicone oil drop	Solid surface	ΔT_c [K] (Wetting)
2 cs	glass	1.5
	copper	1.8
5 cs	glass	2.0
	copper	2.1
100 cs	glass	> 70
	copper	> 70

(*c*) $\Delta p\, R/\sigma = 2.8$

Viscosity of the silicone oil drop	Solid surface	ΔT_c [K] (Wetting)
2 cs	glass	2.1
	copper	2.3
5 cs	glass	2.4
	copper	2.7
100 cs	glass	> 70
	copper	> 70

TABLE III. – Measured critical temperature differences for diesel oils in contact with a copper surface.

$\Delta p\, R/\sigma = 2.8$

Diesel oils	ΔT_c [K] (Wetting)
AGIP	25-27
ESSO	22-24
FINA	20-22
Q8	18-20
SHELL	23-26
IP	24-26

TABLE IV. – Experimental results for the air film thickness and for contact zone extension in the case of silicone oil 5 cs.

Silicone oil 5 cs		$\Delta p\, R/\sigma = 2.8$
Temperature difference ΔT [K]	Equilibrium thickness $h_{eq.}$ [μm]	Contact zone extension [mm]
50	8.0	0.83
25	4.5	0.74
$\Delta T_c = 1.5$ [K]	Not appreciable	0.45

the air gap by means of a background illumination; b) an interferometric technique that provides interference fringes related to the change of the film thickness in the contact region. This second method can only give measurements of the relative path length and then measurements of the relative change of film thickness.

The optical system used for the visualisation of the gap, in the case of a background illumination, is able to obtain magnification on the monitor up to 300 times of the contact region. Figures 4 *a-c* show TV pictures of the air gap between the 1 mm radius drop of silicone oils 5 cs and the solid surface, for different values of the imposed temperature difference (ΔT). The corresponding values of the measured film thickness are reported in Table IV. When ΔT between the upper disk supporting the drop and the wall is very large the gap can be clearly visualised; the film thickness decreases with decreasing temperature differences. Since the relative distance between the upper disk and the solid surface remains unchanged, and the volume of the liquid is constant, the extension of the contact region decreases with ΔT.

The background illumination technique is not able to give quantitative results for temperature differences close to ΔT_c (*i.e.* when the gap becomes of the order of 2-3 μm. An interferometric technique, based on the method described by Francon (1966) and illustrated in Figure 5, has been implemented to measure small film thicknesses. The hot drop is pressed over a glass plate maintained at constant temperature. The glass used is of optical quality, with a constant thickness, within an accuracy at a fraction of the wavelength used. The relative deformation of the glass plate due to the applied pressure (of the order of 10^{-7} Newton/m^2) is negligible.

A laser beam, with wavelength $\lambda = 0.67\ \mu$m and power $w = 12$ mW illuminates the contact region between the drop and the wall. The beam is reflected by the drop surface and projected with a mirror over a white screen. The resulting image consists of a number of almost circular concentric fringes (*Figs.* 6), due to the interference between the rays reflected by the drop surface and those reflected by the upper surface of the glass plate (*Fig.* 7). The fringe position and number can be correlated with contours of equal thickness of the air film between the drop and the solid surface.

The difference of the film thickness (Δh) between two consecutive fringes and the wavelength (λ) of the laser beam (for a laser beam almost orthogonal to the solid surface) are related by:

$$\Delta h = (\lambda/2) \cos i \tag{1}$$

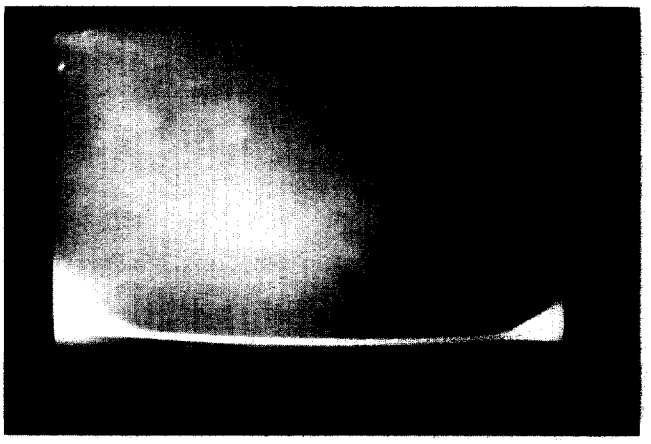

(*a*)

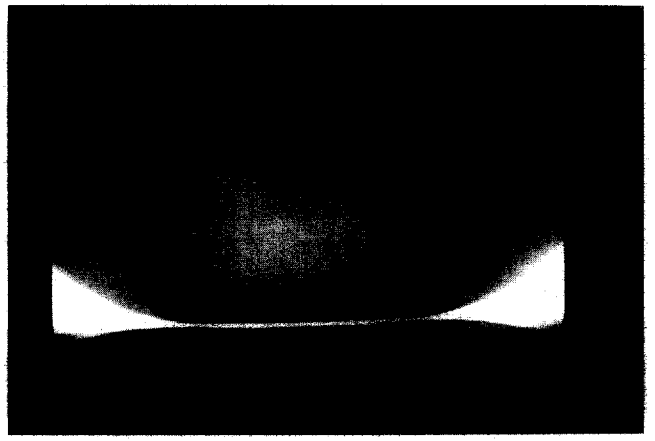

(*b*)

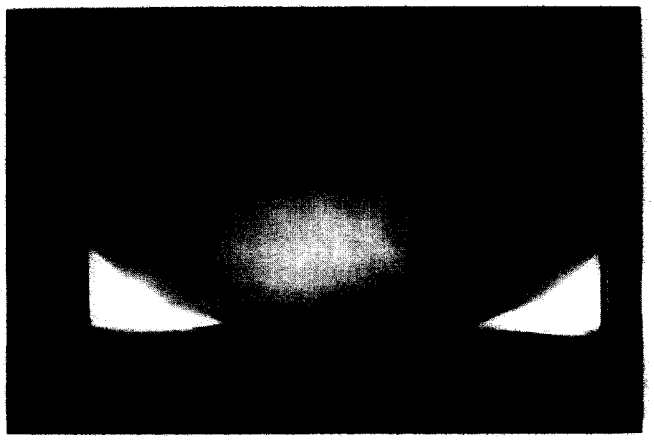

(*c*)

Fig. 4. – Visualization of the film thickness by means of background illumination. (*a*): $\Delta T = 50$ K; (*b*): $\Delta T = 25$ K; (*c*): $\Delta T = 1.5$ K.

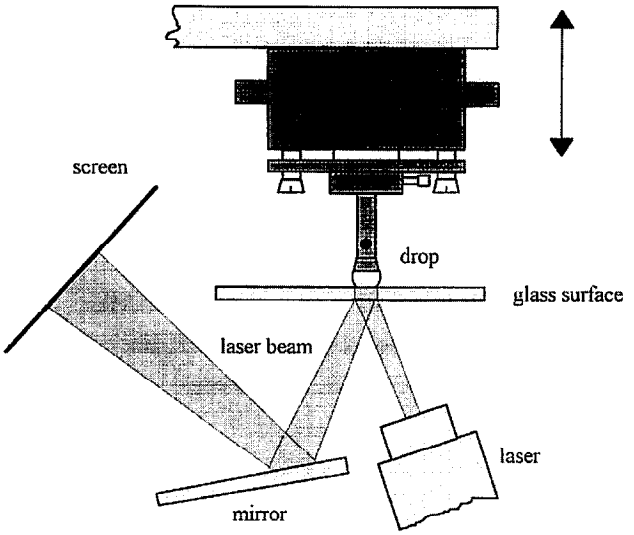

Fig. 5. – Scheme of the experimental apparatus used for the interferometric technique.

where (i) is the angle between the laser beam and the direction normal to the glass plate (see *Fig.* 7). In our experimental measurements this angle was about 6-7 degrees.

Therefore, when passing from the k-th fringe to the $(k+1)$-th fringe, the film thickness increases (or decreases) of about 0.33 μm.

A simple arrangement was designed to calibrate the system (*Fig.* 8). Two glass surfaces have been superimposed with the upper one tilted at a small known angle. Illuminating a narrow portion from below with a laser beam of fixed diameter (d), a number of interference fringes has been obtained, corresponding to the contours of equal thickness of the air layer between the plates. Since the variation between two consecutive fringes is 0.33 μm, the overall change of thickness over this region is given by (see *Fig.* 8):

$$\Delta h = dh/b = N\,0.33\,\mu\mathrm{m} \tag{2}$$

where N is the total number of the fringes that increases proportionally to the angle of inclination (*Fig.* 9).

The interference fringes illustrated in the Figures 6 $(a\text{-}c)$ have been obtained for the same conditions as for the images shown in Figures 4 $(a\text{-}c)$ (*i.e.* for $\Delta T = 50\,\mathrm{K}$, $25\,\mathrm{K}$, $1.5\,\mathrm{K}$). The results confirm that when the imposed temperature difference ΔT is reduced, the extent of the contact region and the thickness of the air film decrease. In fact, the number of fringes, proportional to the overall variation of the film thickness, from the circular wedge to the symmetry axis, is a decreasing function of ΔT. Since the fringes are the contours of equal thickness, it is possible to evaluate the geometrical shape of the drop surface in the contact region, in correspondence of a fixed temperature difference.

In order to determine how the film thickness at a given point changes with time, when the temperature difference is changed, one must measure the number of fringes (n) crossing this point corresponding to a ΔT change. The overall change is obtained multiplying $n \times 0.33$ μm. This procedure has been employed to evaluate the variation

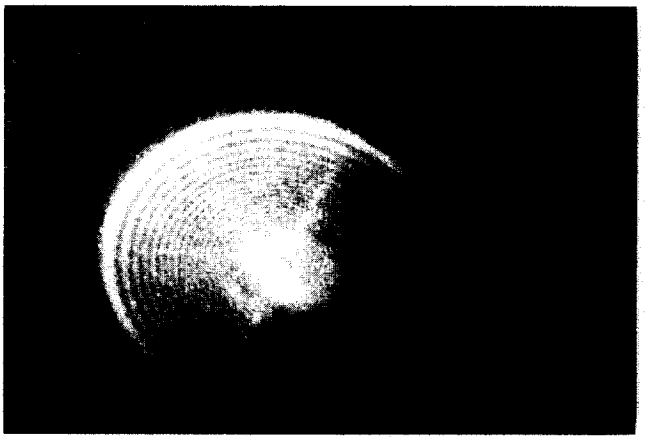

(*a*)

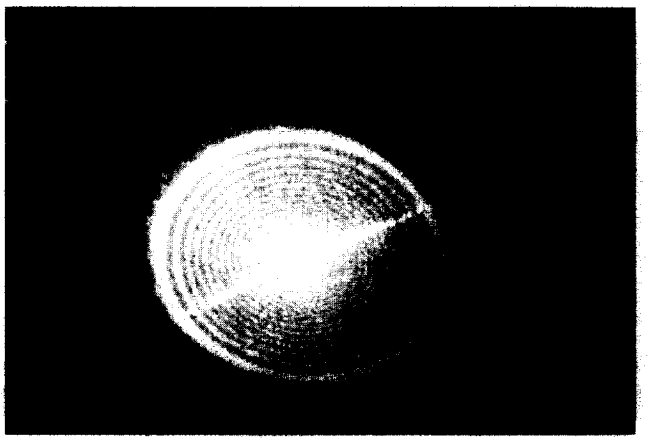

(*b*)

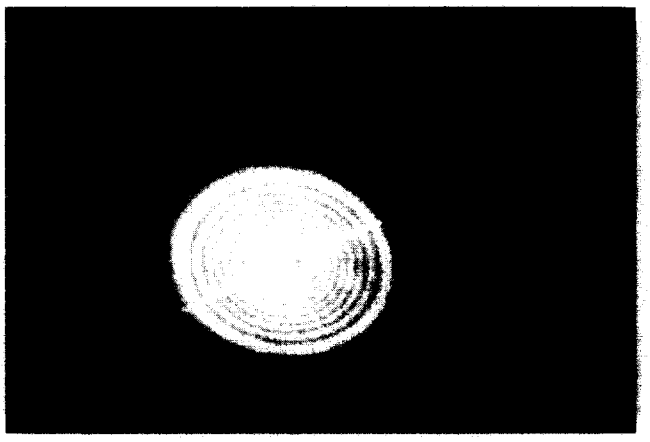

(*c*)

Fig. 6. – Interference fringes observed in comparison with the images shown in Figures 4 (*a-c*).

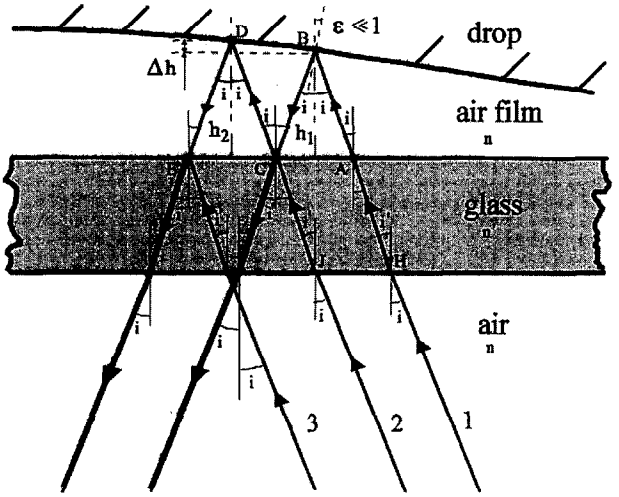

Fig. 7. – Scheme of the optical path leading to the interference fringes.

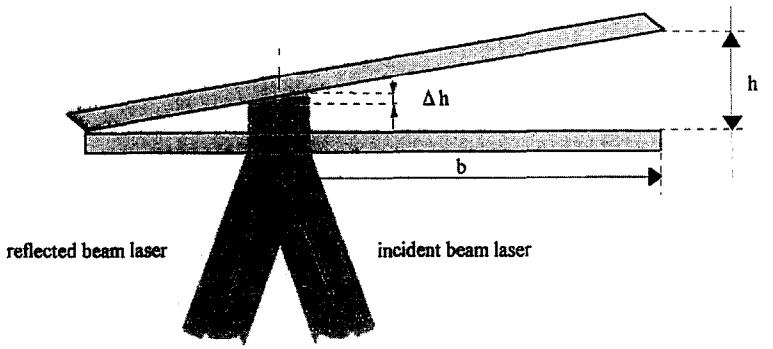

Fig. 8. – Scheme of the experimental arrangment used to calibrate the interferometric technique.

of the air film thickness near the symmetry axis when the temperature difference ΔT between the upper disk and the solid wall is decreased from an initial value of about 70 K until the occurrence of the critical conditions for solid wetting (gap of the order of 1 μm (see *Figs.* 10 *a, b*). In Figure 10 *a* the film thickness is denoted by h and the relative thickness change is $n \times 0.33$ μm.

To get absolute measurements of the film thickness by the interferometric method (which can only yield, as stated, relative measurements) one needs to know the absolute value of the film thickness at least at one point. This is done by relation to a relatively large temperature difference case using the background illumination system, which gives the absolute value of the film thickness with sufficient accuracy at these large temperature differences (e.g. for $\Delta T = 50$ K, $h = 8$ μm); in this way the time history of the film thickness during cooling of the drop can be determined.

This procedure allows one to evaluate the absolute value of the film thickness in relation to the critical temperature difference. In particular, for the configuration corresponding

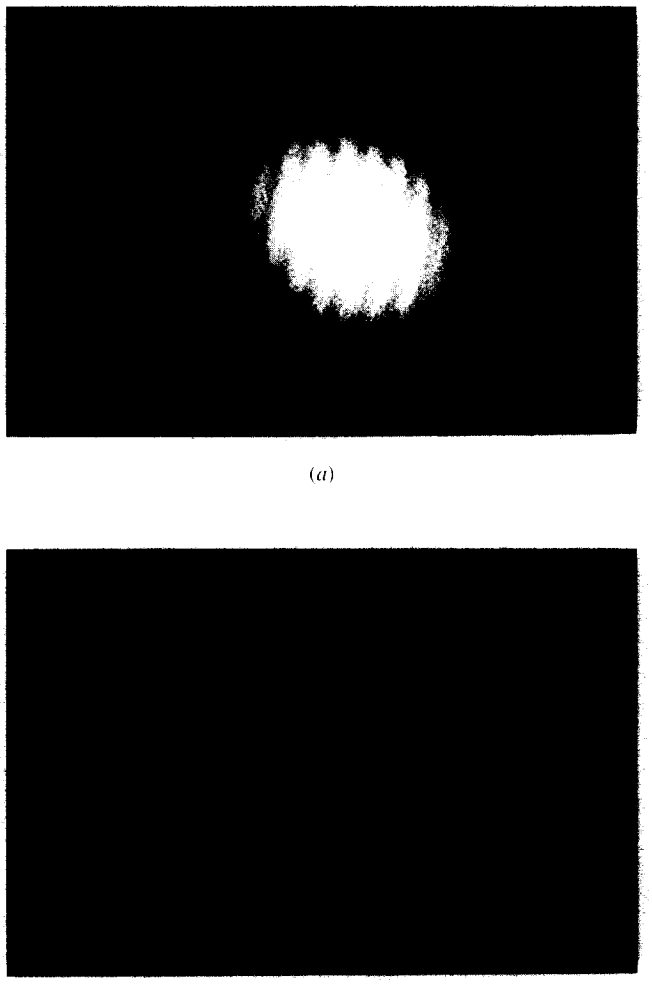

Fig. 9. – Interference fringes observed with the system illustrated in Figure 8.
In Figure 9 *b* the angle between the plates is twice the angle corresponding to the fringes of Figure 9 *a*.

to the images of the Figures 4 and 6, the film thickness immediately before wetting ($\Delta T_c = 1.5$ K) is about $h_c = 1.8$ μm (at $t_c = 240$ s).

3. Numerical modelling

The numerical simulation includes the evaluation of the drop shape, the solution of the flow field inside the liquid drop and the evaluation of the velocity and pressure distributions in the air film between the drop and solid surface.

3.1. Evaluation of the drop shapes

The shape of the drop depends on the relative distance between the supporting disk and the horizontal wall surface. According to the model developed by Savino and Monti

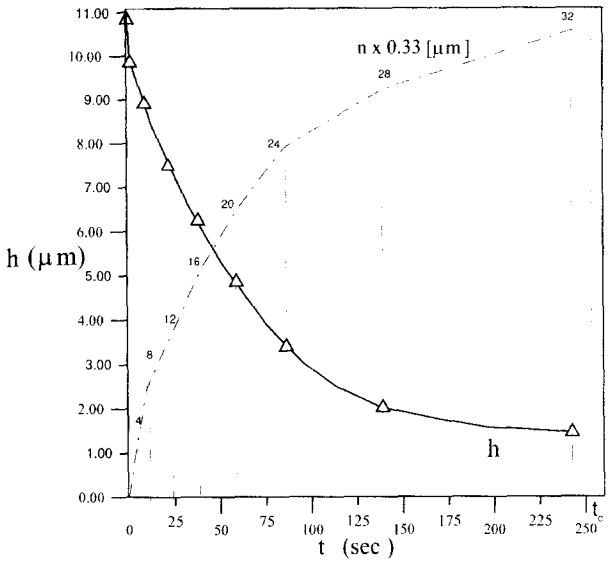

(*a*)

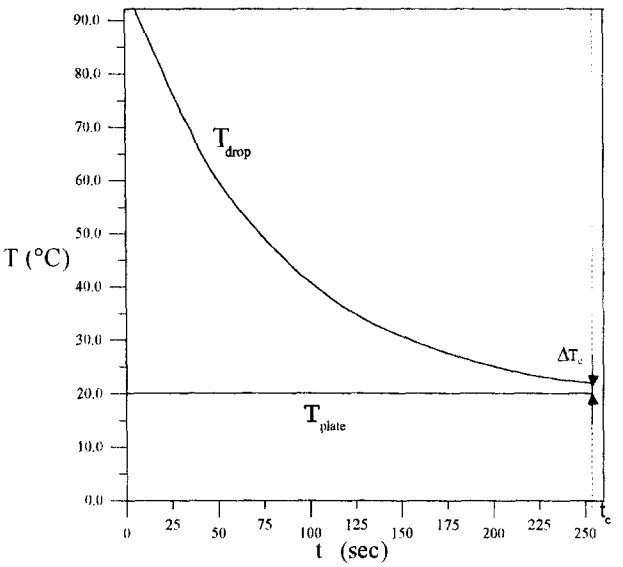

(*b*)

Fig. 10. – Variation with time of the film thickness measured with the interferometric technique (*a*), for a drop of a silicone oil 5 cs. The time histories of the temperatures on the disk and on the plate are shown in Figure 10 *b*. The numbers on the curve $n \times 0.33$ μm (10 *a*) refer to the number of fringe (n) crossing a point near the symmetry axis.

(1997), a constant pressure jump is assumed across the curved portion of the drop surface, from the disk edge ($x = 0$, $r = R$), to the wedge of the contact region ($x = x_c$, $r = r_c$) where $dx/dr = 0$ (see *Fig.* 11).

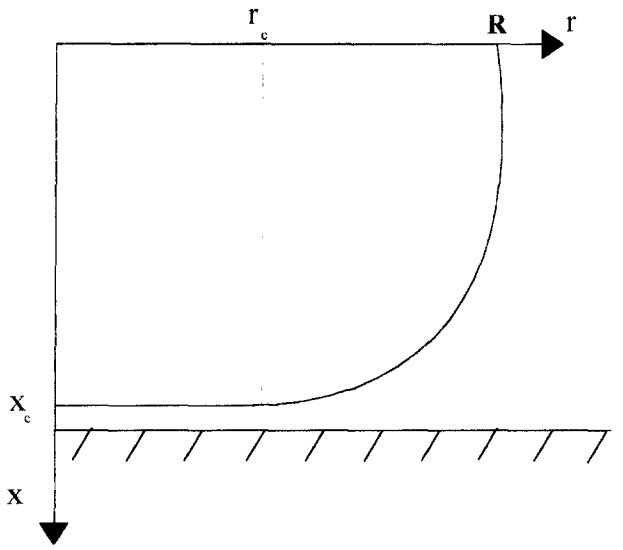

Fig. 11. – Geometry of the problem and co-ordinate system.

It is assumed that the static drop shape is not modified by the presence of the flow (*i.e.* that flow-induced deformations are negligible) and that the contact region is flat in a first order approximation.

Under the above assumptions, neglecting gravitational effects, the shape of the curved drop surface can be obtained from the Gauss-Laplace equation that relates the local curvature of the surface to the pressure jump across the liquid-gas interface:

$$\Delta p = \sigma \left(\frac{1}{R_1} + \frac{1}{R_2} \right) \tag{3}$$

where R_1 and R_2 are the principal radii of curvature at the generic point of the drop surface and σ is the surface tension.

Equation (3) has been solved by a fourth-order Runge-Kutta method, subjected to the conditions: 1) the drop is attached to the upper support at the disk edge; 2) the curved part of the drop surface terminates at the end of the liquid-solid contact region (with a horizontal tangent); 3) the volume of the drop pressed against the solid surface is equal to the volume of a hemispherical hanging drop of radius R.

Figures 12 (*a-c*) show three different computed drop shapes, corresponding to three different values of the dimensionless pressure jump. The origin of the x-axis has been located at the liquid-film flat contact region.

Both the experimental and the numerical data refer to isothermal conditions. However, since the drop shapes are not significantly modified by the presence of the flow (*i.e.* the flow-induced deformations are negligible) these shapes have been used as input geometries for the computation of the flow fields in the liquid drops.

3.2. Fluid dynamic model

The flow and temperature fields are computed on two different domains, *i.e.* the liquid drop and the air layer between the drop surface and the solid wall, and an iterative

procedure, similar to the one described by Savino and Monti (1997) is applied to find the solution.

The equations governing the temperature and velocity fields in the liquid drop and in the air film are the continuity, Navier-Stokes and energy equations:

$$\nabla \cdot \underline{V} = 0 \tag{4}$$

$$\frac{\partial \underline{V}}{\partial t} + \underline{V} \cdot \nabla \underline{V} + \frac{1}{\rho} \nabla p = \nu \nabla^2 \underline{V} \tag{5}$$

$$\frac{\partial T}{\partial t} + \underline{V} \cdot \nabla T = \alpha \nabla^2 T \tag{6}$$

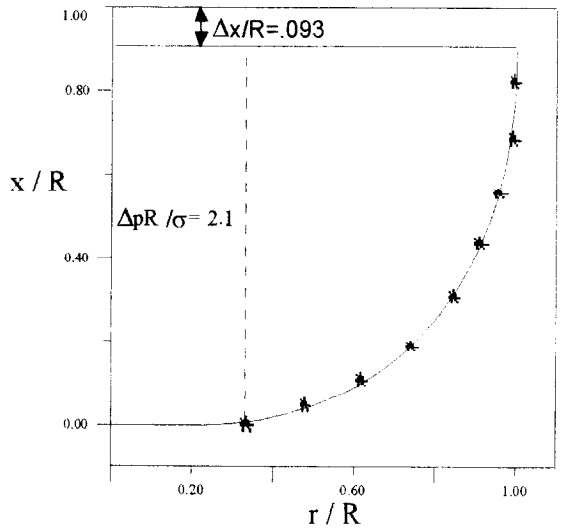

(*a*)

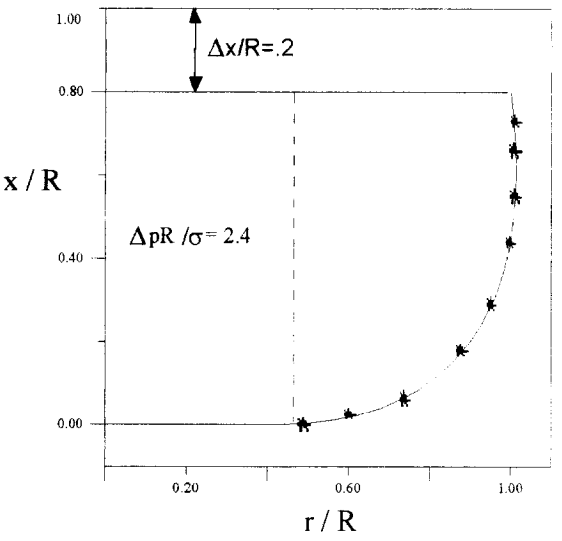

(*b*)

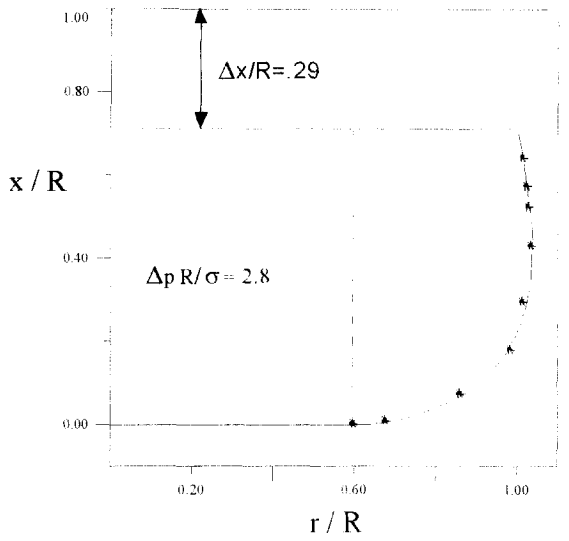

(*c*)

Fig. 12. – Comparison between numerical and experimental results concerning the drop shapes for $\Delta p\, R/\sigma = 2.1$ (*a*), 2.4 (*b*), 2.8 (*c*), corresponding to three different deflections $\Delta x/R = 0.093$, 0.2, 0.29.

where ν is the kinematic viscosity and α the thermal diffusivity.

For the domain corresponding to the liquid drop the boundary conditions are: no slip conditions for the velocity and prescribed constant temperature on the upper support; the Marangoni condition for the velocity and the adiabatic condition for the temperature along the liquid drop surface contacting the ambient air; surface momentum balance and energy conservation along the contact surface in the region of thickness h; symmetry conditions along the axis. Mathematically, with reference to Figures 12:

upper disk $\quad 0 \leq r/R \leq 1;\ x/R = 1 - \Delta x/R$

$$u = 0; \quad v = 0; \quad T = T_{\text{disk}} = T_{\text{hot}} \tag{7}$$

drop surface $\quad r_c/R \leq r/R \leq 1;\ 0 \leq x/R \leq 1 - \Delta x/R$

$$V_n = 0; \quad \mu_l \frac{\partial V_s}{\partial n} = \sigma_T \frac{\partial T}{\partial s}; \quad \frac{\partial T}{\partial n} = 0 \tag{8}$$

contact zone $\quad 0 \leq r/R \leq r_c/R;\ x/R = 0$

$$u = 0 \tag{9}$$

$$\mu_l \left(\frac{\partial v}{\partial x}\right)_l - \mu_a \left(\frac{\partial v}{\partial x}\right)_a = \sigma_T \frac{\partial T}{\partial r} \tag{10}$$

$$\lambda_l \left(\frac{\partial T}{\partial x}\right)_l = \lambda_a \left(\frac{\partial T}{\partial x}\right)_a \tag{11}$$

$$axis\ of\ symmetry\ r/R = 0;\ 0 \leq x/R \leq = 1 - \Delta x/R$$

$$v = 0 \tag{12}$$

$$\frac{\partial u}{\partial r} = 0 \tag{13}$$

$$\frac{\partial T}{\partial r} = 0 \tag{14}$$

where σ_T is the derivative of the surface tension with the temperature, n and s denote the directions orthogonal and tangential to the drop surface, u and v are the velocity components along x and r; the subscripts (l) and (a) refer to the liquid and air phases, respectively.

For the air layer domain the boundary conditions are: no slip conditions for the velocity and prescribed constant temperature on the solid wall:

$$solid\ surface \quad 0 \leq r/R \leq r_c/R;\ x/R = -h/R$$
$$T = T_{\text{plate}} = T_{\text{cold}} \tag{15}$$

the symmetry conditions along the axis (Eqs. 12-14); the velocity and temperature profiles obtained by the numerical solution of the flow inside the drop along the common boundary (contact zone); inflow velocity conditions obtained under the assumptions of viscous parallel flow (Savino and Monti, 1997).

The problem has been solved with the numerical method described by Savino and Monti (1997). The computational domain in the drop was discretized using a mesh of 14 grid points along the drop surface, 20 points along the contact zone and 20 points in the radial direction. For the air layer a mesh with 21 × 81 points was considered.

TABLE V. – Convergence histories for the same conditions of Figure 18.

(*a*) Silicone oil 5 cs $\Delta p\, R/\sigma = 2.1$

N° iteration	$(\Delta p)_m$ [dyne/cm^2]	$\Delta h/R$
0	420	0
1	64	0.0045
2	85	0.001
3	79	0.0028
4	82	0.0020
5	80	0.0025

(*b*) Silicone oil 5 cs $\Delta p\, R/\sigma = 2.8$

N° iteration	$(\Delta p)_m$ [dyne/cm^2]	$\Delta h/R$
0	560	0
1	208	0.045
2	307	0.005
3	283	0.017
4	303	0.008
5	292	0.011
6	300	0.009
7	298	0.010

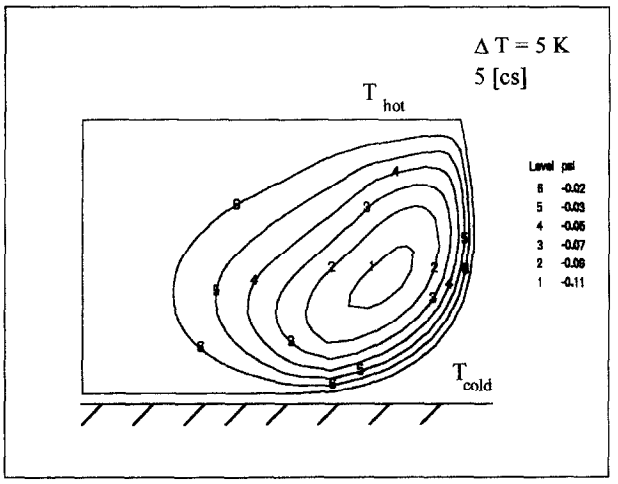

(a)

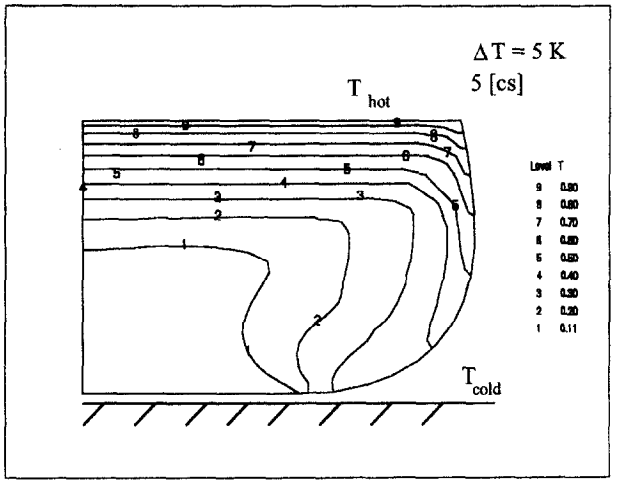

(b)

Fig. 13. – Streamlines (*a*) and isotherms (*b*) in the case $\Delta T = 5$ K for $\Delta p\, R/\sigma = 2.8$ and silicone oil 5 cs.

Once the pressure distribution in the air film has been computed, the shape of the drop in the contact zone is corrected accordingly. Since the pressure distribution depends in turn on the drop shape, this process leads to an iterative process until a solution for the drop shape and for the pressure distribution is obtained. Convergence was typically achieved after 6 or 7 iterations, as shown in Table V, where at each iteration the values of the average pressure jump (Δp_m) are indicated, together with the overall change of the film thickness along the contact region, divided by $R(\Delta h/R)$ (that measures the size of the dimple formed in the gap).

As described by Savino and Monti (1997) the drop shapes show a very small dimple in the stagnation region, so that the solution in the drop is not significantly modified due to the non uniform pressure distribution and to the drop deformation, when compared to the solution obtained under the assumption of planar contact region.

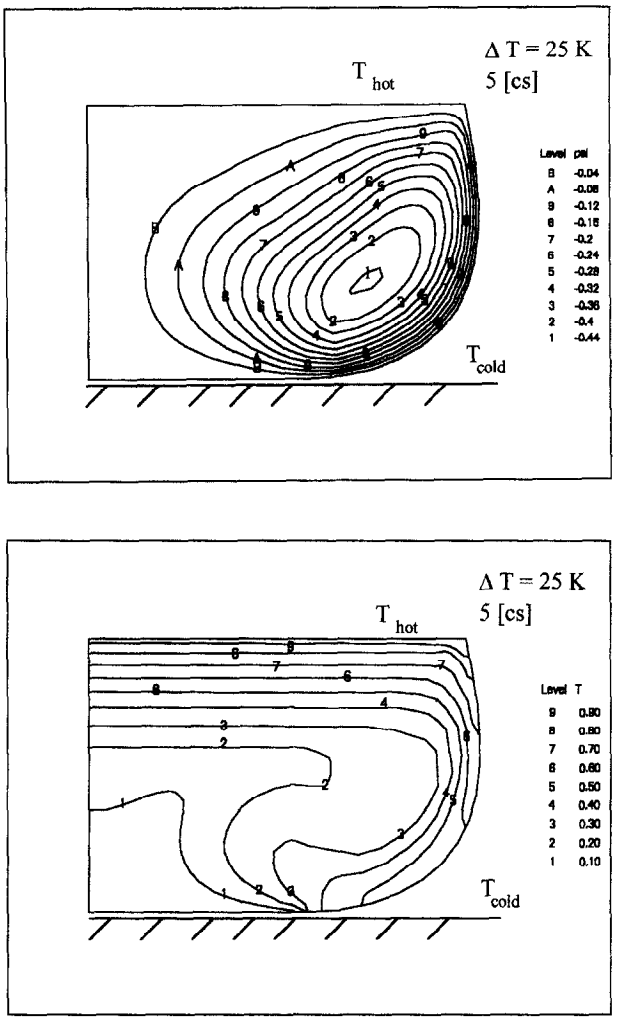

Fig. 14. – Streamlines (*a*) and isotherms (*b*) in the case $\Delta T = 25$ K for $\Delta p\, R/\sigma = 2.8$ and silicone oil 5 cs.

3.3. Numerical results

The numerical simulations have been performed for a drop radius $R = 1$ mm, equal to the radius of the copper disk sustaining the drop during the experimental investigations, and considering the different liquids and the different temperature differences investigated.

Figures 13 show the computed streamlines (*Fig.* 13 *a*) and isotherms ($0 \leq \frac{T - T_{\text{cold}}}{T_{\text{hot}} - T_{\text{cold}}} \leq 1$, *Fig.* 13 *b*) in the case of a drop of silicone oil 5 cs, with a pressure jump $\Delta p\, R/\sigma = 2.8$ and a temperature difference $\Delta T = 5$ K.

The streamlines show the presence of a clock-wise vortex cell. In particular, since the surface tension gradient is opposite to the imposed temperature gradient, the flow along the drop surface is directed from the hot support to the contact region. The computed flow and temperature fields shown in Figures 14 correspond to a temperature difference $\Delta T = 25$ K. In this case the vortex cell is stronger than in the case $\Delta T = 5$ K.

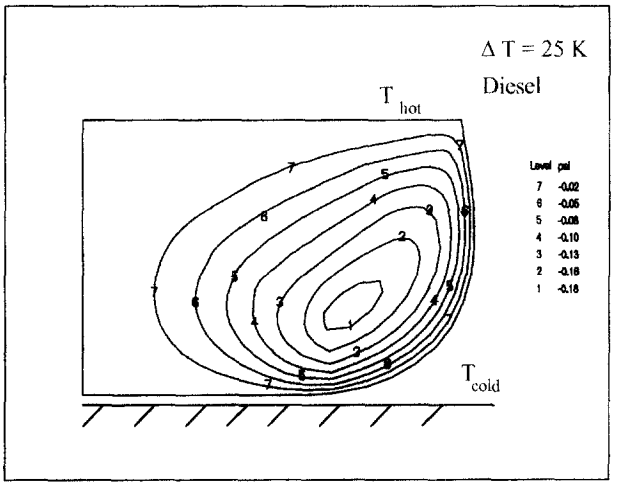

(a)

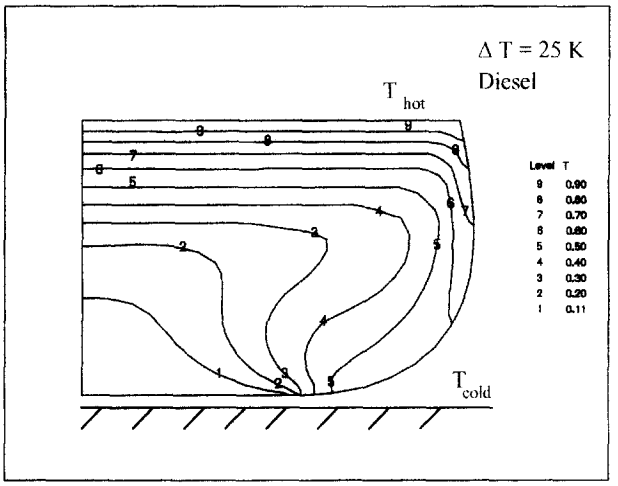

(b)

Fig. 15. – Streamlines (*a*) and isotherms (*b*) in the case $\Delta T = 25$ K for $\Delta p\, R/\sigma = 2.8$ and diesel oil.

Consequently, larger temperature distortions of the isotherms can be observed, compared to the previous case.

The pictures explain how an air film is formed due to the surface velocities at the drop surface, and why this entrainment effect increases when the temperature difference is larger.

The computed fields in the case of a drop of diesel oil, with a pressure jump $\Delta p\, R/\sigma = 2.8$, in the presence of a temperature difference $\Delta T = 25$ K are shown in Figures 15. We must emphasize that for the diesel oil the Marangoni velocities induced by the same temperature difference are smaller than for the silicone oil exhibiting the same viscosity. This is essentially due to a value of the surface tension derivative σ_T smaller for diesel oils than for silicone oils (*see* Table I).

The streamlines and the pressure contours in the air film are shown in Figures 16, for the same experimental conditions of Figures 14. The solution refers to the case of

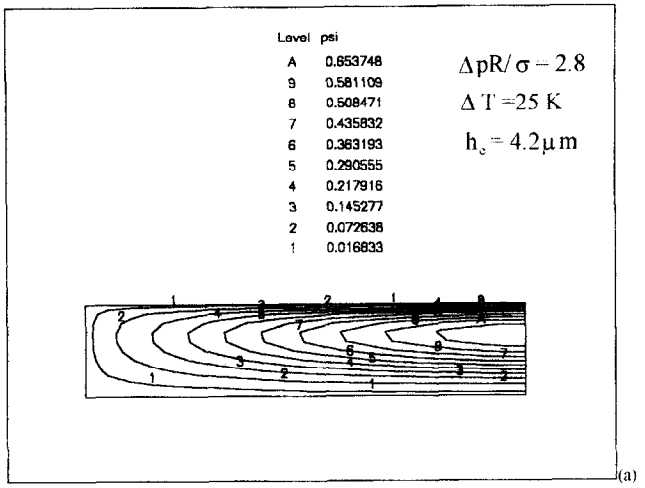

(*a*)

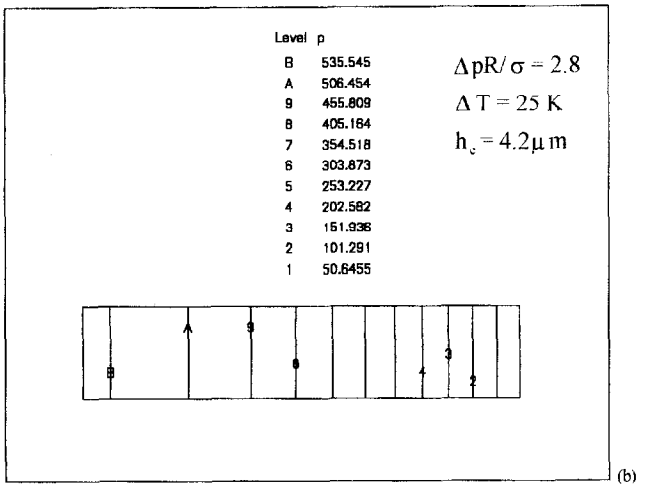

(*b*)

Fig. 16. – Streamlines (*a*) and pressure distribution (*b*) in the air film, for the same conditions of Figure 12 and $h = 4.2$ microns.

planar contact region. To improve the understanding of the axisymmetrical flow field the radial and axial dimensions are not in scale. The tangential viscous stresses in the air film are responsible for the change of the pressure, that gradually increases from the ambient value at the edge of the contact region to the maximum value on the symmetry axis (stagnation point); the pressure difference is of the same order of magnitude as the pressure jump necessary to deform the drops.

As explained before and widely discussed by Savino and Monti (1997) this pressure increase is not consistent with flat contact, which implies constant pressure along the layer.

Therefore, the deflection of the interface, due to the pressure imbalance, is computed using the Gauss Laplace equation, and a new solution is obtained in the modified layer. This method is iteratively applied to find a converged solution (*see* Savino and Monti, 1997).

4. Comparison between experimental and numerical results

An extensive numerical experimentation has been performed to correlate the experimental with the numerical results. In particular, for a given drop shape, corresponding to a given value of the pressure jump across the surface exposed to the surrounding ambient pressure, and for an imposed temperature difference, the equilibrium thickness, for which the pressure in the air film balances the pressure in the liquid drop, has been determined numerically for the different liquids.

All the numerical and experimental results concerning the equilibrium thickness of the gap (h), the dimensionless pressure difference ($\Delta p\, R/\sigma$), the temperature difference (ΔT) and the drops deformations ($\Delta x/R$) are summarised in Tables VI and VII. These tables confirm all the experimental observations both qualitatively and quantitatively. In particular, for a given value of the drop deformation ($\Delta x/R$), the film thickness h increases with the imposed temperature difference, due to the larger entrainment effect caused by stronger Marangoni flow along the liquid drop surface, which in turn produces a larger excess pressure.

For a fixed value of the imposed temperature difference (ΔT), the thickness h decreases when the drop is more deformed, and when the temperature difference is reduced, the same pressure in thc film can be obtained with smaller values of the film thickness.

The numerical behaviour supports the experimental evidence, discussed before, that shows the existence, for a fixed value of the pressure, of a critical temperature difference for the wetting of the solid surface. In fact, in correspondence of the experimentally

TABLE VI. – Summary of numerical results for a drop of silicone oil 5 cs.

Silicone oil 5 [cs]

$\Delta p\, R/\sigma$	$\Delta x/R$	Computed equilibrium thickness h/R					
		$\Delta T = 1.4$ K	$\Delta T = 3.5$ K	$\Delta T = 5$ K	$\Delta T = 10$ K	$\Delta T = 25$ K	$\Delta T = 50$ K
2.1	0.093	1.15E-03	1.45E-03	1.75E-03	2.45E-03	4.20E-03	7.50E-03
2.4	0.2	1.10E-03	1.40E-03	1.70E-03	2.40E-03	4.10E-03	7.20E-03
2.8	0.29	1.05E-03	1.35E-03	1.65E-03	2.35E-03	4.00E-03	7.00E-03

TABLE VII. – Summary of numerical results for a drop of diesel oil.

Diesel oil

$\Delta p\, R/\sigma$	$\Delta x/R$	Computed equilibrium thickness h/R			
		$\Delta T = 17$ K	$\Delta T = 19$ K	$\Delta T = 25$ K	$\Delta T = 45$ K
2.1	0.093	1.15E-03	1.40E-03	1.78E-03	2.80E-03
2.4	0.2	1.10E-03	1.35E-03	1.74E-03	2.75E-03
2.8	0.29	1.05E-03	1.30E-03	1.70E-03	2.70E-03

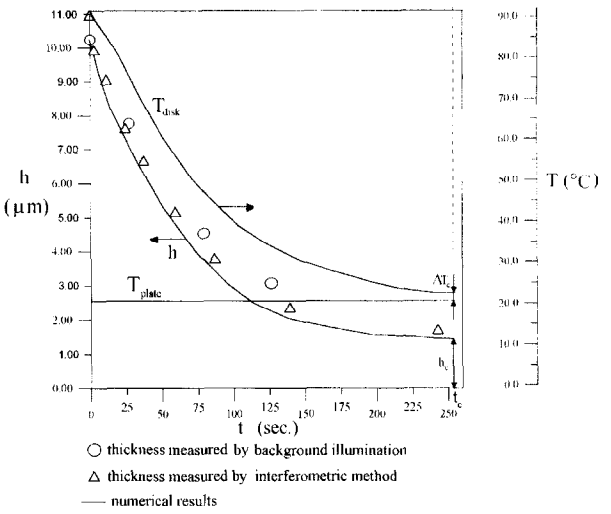

Fig. 17. – Comparison between computed and measured thicknesses of the air film.

measured critical temperature differences, the computed equilibrium thicknesses are all in the range between 1.1 and 1.3 μm. At these distances between the solid wall and the liquid, the drop wets the wall with the consequent formation of the liquid bridge. Since van der Waals forces act at distances one order of magnitude or more smaller than one micron, it is possible that some other instability mechanisms occur, e.g. Rayleigh-Taylor instabilities, causing variations in the interface that allow van der Waals forces to act on a more typical length scale.

In Figure 17 the computed and measured values of the film thickness are compared, in the case of a silicone oil drop with viscosity 5 cs; a very good agreement is found between the numerical and the experimental results. A good agreement is also found comparing the "converged" numerical solution for the shape of the drop in the contact region with the experimental data obtained with the interferometric technique (*Fig.* 18); the presence of a small dimple at the symmetry axis (notice the difference in scale between x and r axis) is found both experimentally and numerically.

5. Conclusions

Wetting prevention between a liquid drop and a solid wall maintained at lower temperatures has been investigated by experimental analysis and numerical simulations. A very intriguing phenomenon was found for the cases in which the temperature of the support sustaining the drop is increased with respect to the temperature of the wall: if the temperature difference exceeds a critical value, the liquid does not spread over the solid. Furthermore if the temperature difference is large enough the drop can be pressed against the solid surface and the liquid surface is deformed like an elastic balloon.

The critical temperature differences for which wetting occurs have been determined experimentally, for silicone oils (with different viscosities) and diesel oils, and for glass and copper surfaces.

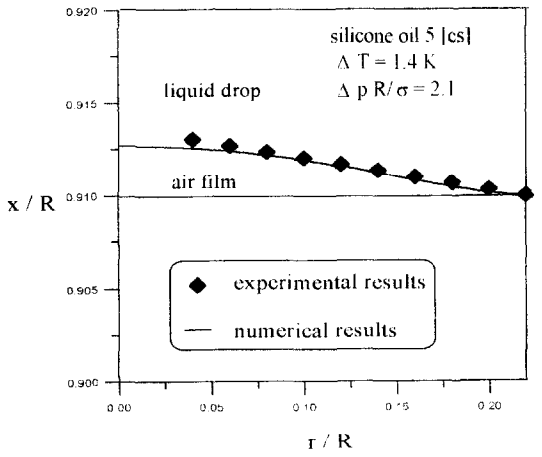

(*a*)

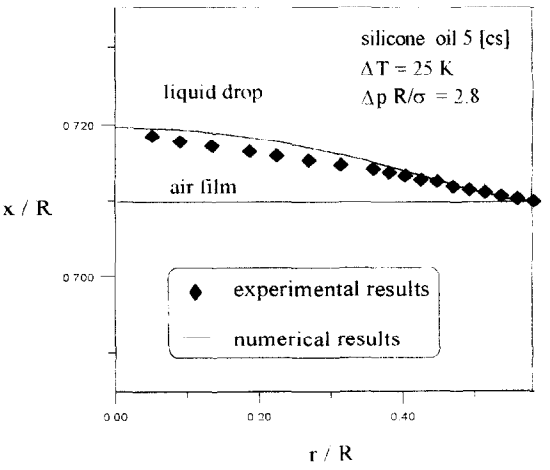

(*b*)

Fig. 18. – Comparison between experimental and numerical results concerning the shape of the drop in the contact region.

The numerical simulation supports the assumption that a thin film of air, separating the drop from the wall, is entrained by the drop surface velocity caused by the Marangoni effect in the liquid drop. The film is thick enough to prevent molecular contact between the liquid and solids surfaces.

A parametric analysis has been performed to determine the thermofluid-dynamic fields in the liquid drops and the air film, for different values of the pressure jump across the liquid drop surface and for different temperature differences.

Good agreement was found between numerical and experimental results. In particular, the computed equilibrium film thicknesses agree with the experimental data, obtained with a background illumination system and with an interferometric technique.

The experimental findings have been correlated by a number of numerically computed parameters (film thickness, shape of the drop, critical temperature differences). Due to the limited size of the drop no local measurement of velocity and temperature is practically possible to complete the study. An experiment on a microgravity platform (sounding rocket, Space Station) will allow the formation of much larger drops (of the order of many centimetres of diameter) and to make possible intrusive and/or non intrusive local measurements of the thermofluidynamic field. A proposal along these lines is being processed.

REFERENCES

AMBROSE J. C., NICHOLAS M. G., STONEHAM A. M., 1996, Dynamics of braze spreading, *Acta Met. Mat.*, **40**, 2483.

ANDERSON D. M., DAVIS S. H., 1995, The spreading of volatile liquid droplets on heated surfaces, *Physics of Fluids*, **7** (2), 248.

BRAUN R. J., MURRAY B. T., BOETTINGER W. J., MCFADDEN G. B., 1995, Lubrication theory for reactive spreading of a thin drop, *Physics of Fluids*, **7** (8), 1797.

DUSSAN V. E. B., 1979, On the spreading of liquids on solid surfaces: static and dynamic contact lines, *Ann. Rev. Fluid Mech.*, **11**, 371.

EHRARD P, DAVIS S. H., 1991, Non-isothermal spreading of liquid drops on horizontal paltes, *J. Fluid Mech.*, **229**, 365.

EHRARD P., 1993, Experiments on isothermal and non-isothermal spreading, *J. Fluid Mech.*, **257**, 463.

FRANCOM M., 1966, *Optical Interferometry*, Academic Press.

FUKAI J., ZHAO Z., POULIKAKOS D., MEGARIDIS C. M., MIYATAKE O., 1993, Modelling of the deformation of a liquid droplet impinging upon a flat surface, *Physics of Fluids A*, **5**, 2588.

FUKAI J., SHIIBA Y., YAMAMOTO T., MIYATAKE O., POULIKAKOS D., MEGARIDIS C. M., ZHAO Z., 1995, Wetting effects on the spreading of a liquid droplet colliding with a flat surface: experiment and modeling, *Physics of Fluids A*, **7**, 236.

GAO F., SONIN A., 1994, Precise deposition of molten microdrops, *Proc. R. Soc. London A*, **444**, 533.

HALEY P. J., MIKSIS M. J., 1991, The effect of the contact line on droplet spreading, *J. Fluid. Mech.*, **223**, 57.

MONTI R., SAVINO R., 1996, Numerical model of non coalescence liquid drops and correlation with experimental results, *Microgravity Quartely*, **6**, 102

MONTI R., SAVINO R., CICALA A., 1996, Surface tension driven-flow in non coalescing liquid drops, *Acta Astronautica*, **38**, 937.

MONTI R., SAVINO R., 1997, Correlation between experimental results and numerical solutions of the Navier-Stokes problems for two non coalescing liquid drops with Marangoni effect, *Physics of Fluids*, **9** (2), 260.

SAVINO R., MONTI R., 1997, Modelling of non coalescing liquid drops in the presence of thermocapillary convection, *Meccanica*, **32**, 115.

SMITH M. K., 1995, Thermocapillary migration of a two-dimensional liquid droplet on a solid surface, *J. Fluid Mech.*, **294**, 209.

TRAPAGA G., MATTHYS E. F., VALENCIA J. J., SZEKELY J., 1992, Fluid flow, heat transfer and solidification of molten metal drops impinging on substrates: comparison of numerical and experimental results, *Metall. Trans. B*, **23**, 701.

YOST F. G., HOSKING F. M., FREAR D. R., 1993, Introduction: The mechanics of solder alloy wetting and spreading, in *The Mechanics of Solder Alloy Wetting and Spreading*, YOST F. G., HOSKING F. M., FREAR D. R. Eds., The Minerals, Metals and Materials Society, Warrendale, PA.

(Manuscript received March 5, 1997;
revised July 17, 1997;
accepted July 23, 1997.)